TABLE III. The global hubs of the structural brain networks

		Young			Middle			Old			
Abbreviations	Class	N_{bc}(i)	Module	Role	N_{bc}(i)	Module	Role	N_{bc}(i)	Module	Role	Reference
SFGmed. L	Association	4.559	IV	R2				4.762	IV	R3	E
MTG. L	Association	4.305	V	R3	3.543	V	R3				B, C, E, F, G
SFGmed. R	Association	3.698	IV	R4							A, C, D, E
MOG. R	Association	3.569	I	R3				2.737	II	R3	A, G
ORBmed. R	Paralimbic	2.876	V	R3	3.451	V	R3				
LING. R	Association	2.865	III	R3	1.945	II	R3				B, G
SMG. L	Association	2.846	I	R3	2.579	I	R3	1.997	I	R3	B
SMG. R	Association	2.496	III	R3	1.853	IV	R3	2.249	I	R3	C
PCUN. L	Association	2.442	III	R3							A, D, G
IFGtriang. R	Association	2.321	I	R3	2.610	I	R3	2.999	I	R3	E, G
ORBmed. L	Paralimbic	2.289	V	R3	2.009	V	R3				C
SFGdor. L	Association	2.261	IV	R2							A, D, E, G
MTG. R	Association	2.162	V	R3	3.631	V	R3				B, C, E, F, G
IFGtriang. L	Association	2.086	I	R3	1.854	I	R3	2.689	I	R3	E, G
PCUN. R	Association	2.050	III	R1							A, D, G
SFGdor. R	Association	2.028	IV	R4	1.941	IV	R2				A, C, D, E, F, G
ANG. R	Association							3.431	II	R3	B
AMYG. R	Paralimbic							3.389	V	R3	
PHG. R	Paralimbic							2.760	V	R2	E, F
STG. R	Association				2.986	I	R3	2.665	I	R4	B, C, G
ANG. L	Association							2.318	II	R3	B
INS. L	Paralimbic							2.211	I	R2	D
MOG. L	Association							2.016	II	R3	A, G
THA. L	Subcortical							1.948	I	R3	
STG. L	Association				1.991	I	R1				B, G
ORBinf. L	Paralimbic				3.037	V	R1				B, C
ORBinf. R	Paralimbic				3.018	V	R3				B

The hub regions (normalized node betweenness, Nbc(i)>mean + SD) in structural brain networks of three age groups are listed in decreasing order of the node betweenness in the young group. The regions are classified as association, primary, limbic/paralimbic or subcortical regions as described by Mesulam [2000]. The module column indicates the anatomical modules that the hub regions belong to, and the role column indicates the roles that the hub regions play in terms of their intra- and inter-module connectivity patterns; connector hub (R1), provincial hub (R2), connector non-hub (R3), and provincial non-hub (see Materials and Methods). R: right; L: left. For the description of the abbreviations, see supplementary Table S1.

The reference column indicates the hub regions previously identified in human brain structural (A, B, C, D, E), or functional (F, G) networks. A; Gong et al. [2009], B; He et al. [2008], C; Chen et al. [2008], D; Iturria-Medina [2008], E; He et al. [2007], F; He et al. [2009b], G; Achard et al. [2006].

among the age-specific groups. Using the fixed cost threshold (cost = 0.11), the obtained brain networks that captured the structural connectivity backbone underlying the principal topological organization were separated into modules according to the spectral method proposed by Newman [2006a]. As a result, the brain networks were separated into five, six, and five modules in young, middle, and old groups, respectively (Table IV, see Supporting Information Table SIV). The brain regions included in modules with three age groups were described in Supporting Information Text S1. The surface representations for modules in structural brain networks are shown in Figure 3. Moreover, the modular organization of structural brain networks shown here was also reproduced by using different specific cost thresholds (cost = 0.15 and 0.20), (see Supporting Information Fig. S2). We showed the modular organization of the structural brain networks in topological spaces (Fig. 4A–C). The topological representations were drawn by the Pajek software package (http://vlado.fmf.uni-lj.si/pub/networks/pajek) using a Kamada-Kawai algorithm [Kamada Kawai, 1989]. With this algorithm, the geometric distance between two brain regions on the drawing space approximates the shortest path length between them.

In this study, according to the patterns of intra- and inter-module connections, the four possible roles of regions were defined as connector hub (R1), provincial hub (R2), connector non-hub (R3), and provincial non-hub (R4). To show the node roles of regions in each module, we arranged the connector nodes (R1 and R3) in a central ring. In the young and middle group, 49 regions (8 R1 and 41 R3) and 49 regions (7 R1 and 42 R3) were identified as connector nodes (Table IV, Fig. 4D,E). However, only 28 regions (3 R1 and 25 R3) were defined as the connectors

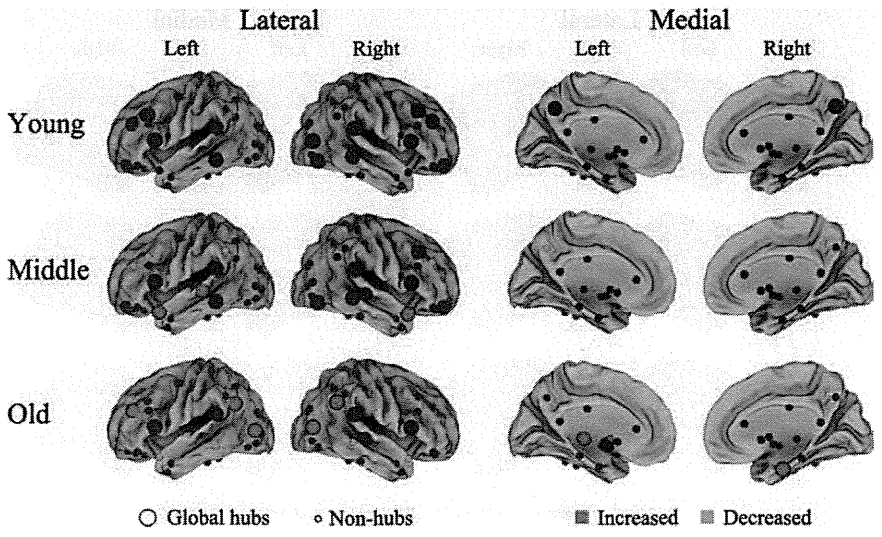

Figure 2.

Surface representations for global hubs and the significant age-related changes in node betweenness. Top: The global hubs in the young group. Middle: The global hubs in the middle group and the significant age-related changes in node betweenness from young to middle age. Bottom: The global hubs in the old group and the significant age-related changes in node betweenness from middle to old age. The global hubs and non-hubs are indicated by spheres in big and small size, respectively. The nodes with significant decreased and increased age-related changes are indicated by green and red spheres, respectively. The nodes without significant age-related change are indicated by blue spheres.

(Table IV, Fig. 4F). Most global hubs (Young, 12/16; Middle, 13/14; Old, 11/14) played R1 or R3 (connector) roles, with numerous inter-module connections executing a critical impact on the coordination of information flow through the whole network (Table III).

In addition to discrepancies in the composition and numbers of modules, we also found differences in the topological roles of the modules in the brain networks of three groups. We defined the connector-module as the module that had both a high connector ratio (the ratio of the connectors to the regions in the module was larger than 0.6) and a high ratio of intermodule connections (the ratio of the intermodule connections in the modules to that in the whole network was larger than <1/numbers of modules>) (Table IV). In both the young and the middle group, Modules I, III, and V were identified as the connector-modules (Table IV). The young brain network was observed to have dense inter-module connections between Module I and V (53/109), as well as between Module I and III (25/109) (see Supporting Information Table SV). In

TABLE IV. The distribution of connectors and inter-module connections in each module

	Young			Middle			Old		
Module	Regions	Connector	Intermodule	Regions	Connector	Intermodule	Regions	Connector	Intermodule
I	16	***11(0.69)***	***80(0.37)***	13	***9(0.69)***	***49(0.25)***	26	7(0.27)	51(0.36)
II	21	8(0.38)	16(0.07)	18	6(0.33)	25(0.13)	10	4(0.40)	43(0.30)
III	14	***12(0.86)***	***43(0.20)***	18	***12(0.67)***	***35(0.18)***	8	4(0.50)	12(0.09)
IV	20	3(0.15)	10(0.05)	19	6(0.32)	16(0.08)	18	6(0.33)	19(0.13)
V	19	***15(0.79)***	***69(0.32)***	14	***11(0.79)***	***58(0.30)***	28	3(0.11)	13(0.09)
VI				8	5(0.63)	15(0.08)			
Total number	90	49	109	90	49	99	90	24	69

The "Connector" column indicates the numbers of connector nodes in each module and its ratio to the total number of regions in the module (in parentheses). The "Intermodule" column indicates the numbers of intermodule connections in each module and its ratio to the total number of intermodule connections in the whole network (in parentheses). The bold and italic characters indicate the values of the connector-module in each age group, with both the higher connector ratio (>0.6) and the higher ratio of intermodule connections (larger than <1/number of modules>).

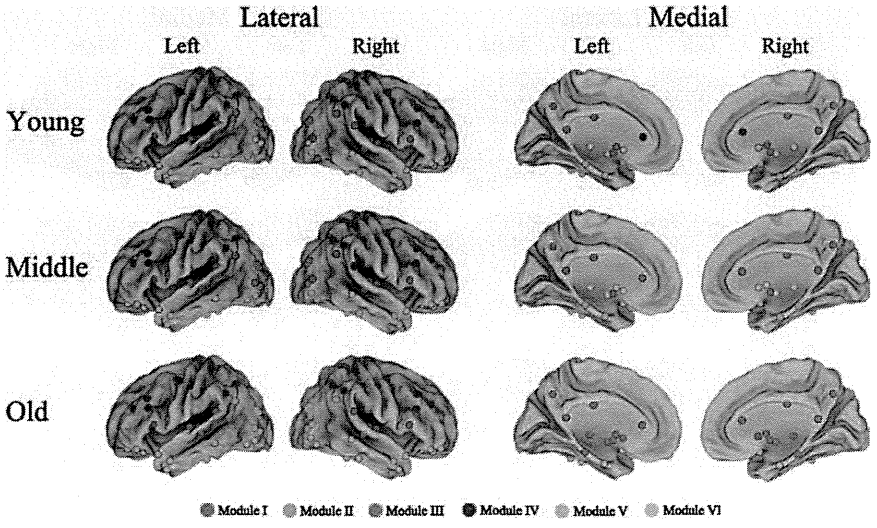

Figure 3.
Surface representations for modules in structural brain networks. All of 90 brain regions are plotted by different colored spheres (different colors represent distinct network modules) and further mapped onto the cortical surfaces at the lateral and medial views, respectively.

the middle group, the inter-module connections spread around modules and abundant connections existed only between Modules I and V (28/99) (see Supporting Information Table SVI). Although no module was recognized as the connector-module in the old group, there were relatively dense inter-module connections between Modules I and II (32/69) (see Supporting Information Table SVII). Furthermore, the young and middle groups showed significantly higher proportions of intermodule connections than did the old group (ANOVA, $P = 0.007$), (Fig. 5).

DISCUSSION

This is the first study, to our knowledge, to investigate both small-world properties and modularity of structural brain networks in healthy individuals across a broad age range. We found that structural brain networks exhibited economical small-world properties in three age-specific groups. We defined the global hubs to account for higher node betweenness in each group. In particular, the small-world properties and node betweenness showed significant changes with normal aging. Moreover, our results demonstrated that structural brain networks showed modular organization in three groups and changed greatly in the old age group. Structural brain networks developed into a more distributed organization from young to middle age, then organized into a localized organization with substantial alterations in old age. Thus, understanding changes in topological properties in structural brain networks may help elucidate normal processes of brain maturation and senescence.

Economical Small-World Properties and Age-Related Changes

In this study, structural brain networks exhibited economical small-world properties in all age-specific groups, as determined using RGMV with MR images. Our findings of high global and local efficiency in structural brain networks with three age-specific groups were compatible with previous functional and structural brain networks studies [Achard and Bullmore, 2007; Bassett et al., 2008; He et al., 2008, 2009a; Wang et al., 2009b]. Computational modeling simulations [Sporns et al., 2000] and experimental studies [Chen et al., 2008] have also suggested the emergence of small-world topology when networks are evolved for the great complexity of dynamic behavior, defined as an optimal balance between local specialization and global integration [Strogatz, 2001]. Thus, our results provided further support for the standpoint that brain networks might have evolved to maximize the cost efficiency of parallel information processing.

We also noted age-related changes in efficiency metrics of structural brain networks. First, the structural brain network may develop into a more distributed organization from young to middle age, accompanied by significant decreases in local efficiency and robust increases in global efficiency. The reduction of local efficiency might be related to that healthy aging is associated with a regionally distributed pattern of gray matter atrophy [Bergfield et al., 2010]. Moreover, a previous study suggests that high global efficiency assures effective integrity or rapid transfers of information between and across remote regions that are believed to constitute the basis of cognitive

process [Sporns and Zwi, 2004]. Recent studies also demonstrate a positive correlation between the global efficiency of brain networks and intellectual performance, indicating a more efficient parallel information transfer in the human brain [Li et al., 2009; van den Heuvel et al., 2009]. Thus, the period from young to middle age may reflect a maturation process in the structural brain network. This finding was also in accordance with that the age-related cognitive changes involved in the age-related loss of gray matter volume [Hedden and Gabrieli, 2004; Resnick et al., 2003; Tisserand et al., 2004]. Second, the structural brain network may evolve into a more local organization from middle to old age. The local efficiency did not differ significantly between the middle and old groups (Fig. 1A), whereas the integrated local efficiency increased significantly (Fig. 1C). Besides, the global efficiency and the integrated global efficiency decreased significantly (Fig. 1B,D). This phenomenon may indicate a degeneration process in the structural brain network with normal aging. It has been suggested the regular networks have a slow signal propagation speed and synchronizability in comparison to small-world networks [Strogatz, 2001]. The regular configuration that upsets the optimal balance of a small-world network was related to many neurological and psychiatric disorders described as dysconnectivity syndromes [Catani and ffytche, 2005]. Many previous studies have reported the regular configuration of brain networks in patients with diseases such as schizophrenia or AD, derived from fMRI, EEG or structural MRI data [Bassett et al., 2008; He et al., 2008; Stam et al., 2007]. There seems to be convergent evidence from methodologically disparate studies that both AD and schizophrenia are associated with abnormal topological organization of structural and functional brain networks [Bullmore and Sporns, 2009]. Thus, our results suggested that aging has high risk for dysconnectivity syndromes. Third, the U-curve model defined in this study indicated a quadratic curve-like tendency of structural brain networks with normal aging. Our recent study demonstrated that gray matter volume declined with age in healthy community-dwelling individuals, whereas the white matter ratio (WMR) had an inverted-U curve trajectory with age. WMR increased until around 50 years of age and then decreased in each gender [Taki et al., in press]. This increase in the WMR is thought to represent maturational changes such as myelination, which may continue until middle adulthood. There are other supporting evidences that both gray and white matter magnetization transfer ratio (MTR) histograms follow quadratic curves: in both cases, they increase up until middle adulthood and then decline significantly, as determined by a study that assessed age-related MTR histogram measurements in healthy subjects (54 healthy volunteers Aged 20–86 years), [Ge et al., 2002a,b]. Brain maturation includes both regressive cellular events (such as synaptic pruning) and progressive cellular events (such as myelination), which could result in the appearance of regional gray matter volume decline or cortical thinning on MR images [Sowell et al., 2003, 2004]. It has been noted that brain maturational change continues to about the fifth decade of age [Sowell et al., 2003], which may account for the maturation of structural brain networks.

In addition to the above findings, we observed that the young group showed higher local efficiency (Fig. 1A,C) but lower global efficiency (Fig. 1B,D) as compared with the old group. This finding was different from the results of a previous study [Achard and Bullmore, 2007], in which the young group (N = 15; mean age = 24.7 years) showed higher values in the relative global efficiency and no significant difference in the relative local efficiency compared with the old group (N = 11; mean age = 66.5 years). The discrepancies could be attributed to different network modalities (structural vs. functional) and population size (350 vs. 11/15).

Regional Nodal Characteristics and Age-Related Changes

Node betweenness is an important metric that can be used to determine the relative importance of a node with a network and identify the pivotal nodes in the complex network. As indicated by the higher values of node betweenness, 16, 14, and 14 global hubs that are crucial to efficient communication were identified in the young, middle, and old groups, respectively. These global hub regions were mainly composed of recently evolved association and primitive limbic/paralimbic regions. Association regions have proven to contribute to the integrity of multiple functional systems, such as attention and memory systems [Mesulam, 1998], and tend to be hubs of the brain functional network regardless of age [Achard and Bullmore,

Figure 4.

Modular organization of structural brain networks. Left: The modular organization of young (**A**), middle (**B**), and old (**C**) brain networks visualized by minimizing free energy using a Kamada-Kawaki layout algorithm. The global hubs and non-hubs are represented by the bigger and smaller circles, respectively. The regions are represented by the module color. The intramodule and intermodule connections are represented by the light gray and black lines, respectively. Right: The regional node roles in brain modules for young (**D**), middle (**E**), and old (**F**) brain networks, with connector nodes located in a central ring to highlight intermodule connections. The intramodule and intermodule connections are shown in colored and black lines, respectively.

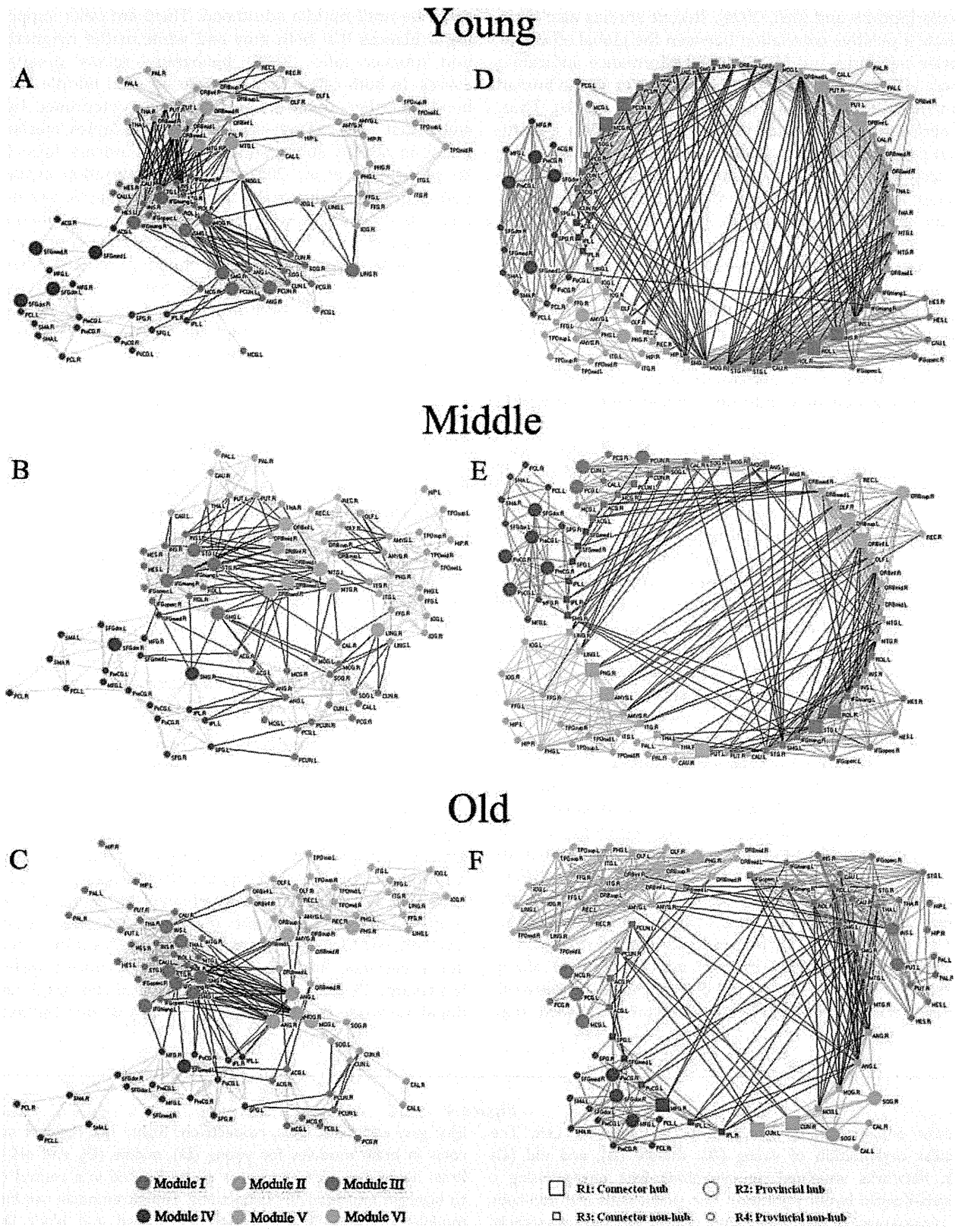
Young
A
D
Middle
B
E
Old
C
F
Module I
Module II
Module III
Module IV
Module V
Module VI
R1: Connector hub
R2: Provincial hub
R3: Connector non-hub
R4: Provincial non-hub

Figure 4.

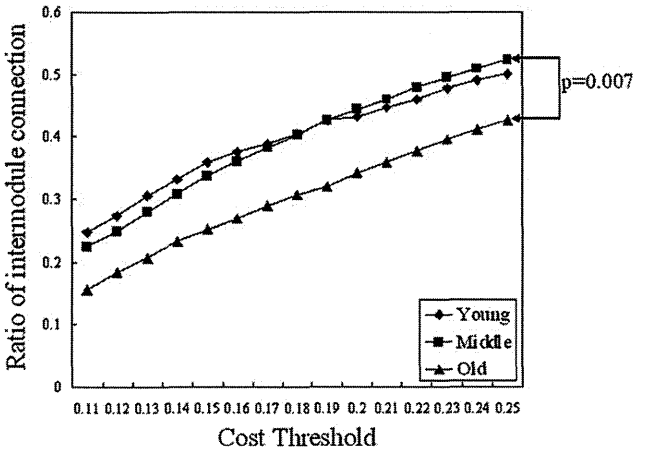

Figure 5.
The ratio of intermodule connections.

2007]. Limbic/paralimbic regions have been shown to be highly interconnected with the prefrontal regions and subcortical regions, and are mainly involved in emotional processing and the maintenance of a conscious state of mind [Mesulam, 1998]. In this study, most global hubs were frontal and parietal regions, especially in the young (12 of 16) and middle (9 of 14) groups. Previous studies have also demonstrated that identified global hubs were mainly prefrontal and parietal regions, providing a potential explanation for their well-documented activation by many cognitive functions [Bullmore and Sporns, 2009]. Moreover, although the identified global hubs varied among three age-specific groups, most of these regions were found to show high regional efficiency or node betweenness in the structural [Chen et al., 2008; Gong et al., 2009b; He et al., 2007, 2008; Iturria-Medina et al., 2008] and functional [Achard et al., 2006; He et al., 2009b] human brain networks (Table III). It was noted that the substantial discrepancies of identified global hubs between this study and the previous studies could be due to the different neuroimaging modalities, subjects' characteristics and computational methods.

We also found significant changes in node betweenness with decreasing and increasing in both periods (see Fig. 2). This finding was consistent with a previous study which indicates both negative and positive age effects on the regional efficiency in cortical regions [Gong et al., 2009a]. The most of these identified regions were association cortices (7 out of 9) in the period from young to middle age. From middle to old age, the regions were association (7 out of 14) and paralimbic/subcortical (7 out of 14) regions. These results supported the view that age-related changes are mainly characteristic of association cortex as opposed to primary cortex [Albert and Knoefel, 1994]. Our results were also similar to the result by a previous study that old age is associated with significantly reduced nodal efficiency in several regions of the frontal and temporal neocortex [Achard and Bullmore, 2007]. We also tried to interpret this phenomenon by previous results in the dynamic course of brain maturation. A previous study indicates that relative regional differences in cortical GM volume with age occur in the frontal, parietal and temporal lobes [Smith et al., 2007]. Importantly, the discrepancies in node betweenness between middle and old groups were more notable than those between young and middle groups (see Fig. 2). Thus, our results suggested that the organization of structural brain networks changed slightly from young to middle age, whereas it altered greatly from middle to old age.

Modularity and Age-Related Changes

Our results indicated the existence of modular organization in the structural brain networks in three age-specific groups. The organization consisted of modules of tightly connected brain regions. Each module in a network has intramodule connections that are denser than its intermodule connections. High local clustering represents a general organizational principle throughout many larger-scale brain networks and may contribute to the balance between brain functional segregation and integration while conserving connection length, efficient recurrent processing within modules, and efficient information exchange between modules [Bassett and Bullmore, 2006; Chen et al., 2008; Latora and Marchiori, 2001; Sporns et al., 2000]. Thus, this finding of modular organization in structural brain networks was consistent with the pre-stated results of economical small-world attributes, indicated by higher local and global efficiency than comparable random and regular networks, respectively. Moreover, we noted that the structural brain networks were organized with topological modules that closely overlap known functional domains such as auditory and language (Module I in young and middle), memory and emotion processing (Module II in young and middle), visual and "default" network (Module III in young and middle), motor and somatosensory (Module IV in young, middle, and old), cognitive processing and learning (Module V in young), and decision-making (Module V in middle). The modules in the old group were quite different from those in the young and middle groups. Specially, Module I was primarily associated with memory, as well as auditory and language functions; Module II was mainly involved in the visual system; Module III was involved with emotion formation and processing; Module V was similar to Modules II and V in the middle group, which were mainly associated with memory, emotion, and cognitive processing. These results were also in accordance with several recent studies on the modular organization of human brain that utilized structural and functional network analyses [Chen et al., 2008; Hagmann et al., 2008; He et al., 2009b]. For the full discussion, see Supporting Information Text S1.

We also found no significant difference with regard to the modularity of the global brain networks among three age-specific groups [see Supporting Information Fig. S1]. This finding was consistent with that of a previous study, in which no significant difference was found between the young and old groups with regard to modularity, implying that modular organization is conserved over the adult age range considered [Meunier et al., 2009a]. Nonetheless, there were notable discrepancies in the composition and topological roles of modules among brain networks in this study. First, comparing the composition of the modules among three age groups, we found that the modular organization of the young and middle groups were very similar but quite different from that of the old group (Figs. 3 and 4). A new module (Module VI) in the old group represented the separation of all subcortical regions from the areas known as Modules I and V in the young group. The constitution of the modules in the middle group resembled that in the young group (see Fig. 4). However, the regions in the old group were assembled more densely, leading to the overnumbered regions in modules (see Fig. 4). This finding may indicate that the modular organization of structural brain networks changes greatly until old age. Second, the number of connectors in the old group was also less than that in the young and middle groups (Table IV). The connectors were crucial for the global coordination of information flow in the brain networks and were of great importance for maintaining network integrity [He et al., 2009b; Sporns et al., 2007]. Moreover, the modules in the old group seemed to be more locally organized, resulting in fewer intermodule connections as compared with the numbers in the young and middle group (see Fig. 5). The intermodule connections facilitate communication between different modules and contribute to the network bridges that serve as pivotal connections for the information flow of the whole brain network [Chen et al., 2008; He et al., 2009b]. This finding was in accordance with a previous study on age-related changes in modular organization of human brain functional networks, in which the number of intermodule connections to frontal modular regions was significantly reduced in an old group [Meunier et al., 2009a]. As a result, three connector-modules were identified in both the young and middle groups, whereas no connector-module was found in the old group (Table IV). The connector-module may play a critical role in coordinating activity across the brain network as a whole and in mediating interactions between modules [Meunier et al., 2009a]. Combined with the findings in the small-world properties and node betweenness, these results may reveal that the structural brain network changed slightly, shifting into a more distributed organization during the transition from young to middle age, and then organizing into a localized organization with great alteration in old age. Our findings were also in agreement with a recent study on functional brain networks, which indicated the organization of multiple functional networks shifts from a local anatomical emphasis in children to a more "distributed" organization in young adults over development [Fair et al., 2009].

METHODOLOGY

The human brain structural network was first constructed by using cortical thickness measurements [He et al., 2007], because of strong correlations between regions that are axonally connected [Lerch et al., 2006]. We used the measurement of RGMV to construct structural brain networks, as applied first by a previous study on the hierarchical organization of human cortical networks [Bassett et al., 2008]. Although there is still no direct proof that correlations of gray matter volume across subjects are indicative of axonal connectivity via white matter tracts, strong correlations between brain regions known to be anatomically connected have been observed in previous optimized voxel-based morphometry studies [Mechelli et al., 2005; Pezawas et al., 2005]. Thus, the RGMV as the measurement of structural connectivity is currently considered as exploratory and should be investigated further in future studies. Salvador et al. showed that regional volume had a positive correlation which its mutual information that measured the functional connectivity between the region and the rest brain regions [Salvador et al., 2008]. A previous study also indicates that network properties (e.g., small-worldness and degree distribution) change with the alterations of topological organization introduced by the different parcellation schemes [Wang et al., 2009a]. Thus, the comparison of network parameters across studies must be made with reference to the spatial scale of the parcellation schemes [Zalesky et al., 2010]. While this study was a cross-sectional study, a longitudinal analysis would also be useful to investigate the change in structural brain networks with normal aging. Because all subjects in this study were more than 20 years old, young and adolescent subjects are expected to be included in future studies of brain network development. It is also important to investigate the topological properties and modular organization of human brain networks with normal aging, in combination with functional and structural studies.

CONCLUSION

In this study, we quantitatively analyzed the changes in small-world properties and modularity of structural brain networks with normal aging, using the structural MRI. Our results indicated that normal aging had a notable effect on the topological organization of structural brain networks. These findings were compatible with previous studies on the small-world and modular organization of brain functional and structural networks, thus enhancing our understanding of the underlying physiology of normal aging in the human brain.

ACKNOWLEDGMENTS

The authors are grateful to the anonymous referees for their significant and constructive comments and suggestions, which greatly improved the article. The brain MRI database was constructed at the Aoba Brain Imaging Center with a grant from the Telecommunications Advancement Organization (National Institute of Information and Communications Technology) of Japan. The work in the present study had been partially reported at the 7th International Symposium on Nano-Biomedical Engineering, October 16–17, 2008, National Cheng Kung University, Tainan, Taiwan; and at the 4th Asian Pacific Conference on Biomechanics, April 14–17, 2009, University of Canterbury, Christchurch, New Zealand. The authors thank American Journal Experts (http://www.journalexperts.com/) for English editing and proofreading.

REFERENCES

Achard S, Bullmore E (2007): Efficiency and cost of economical brain functional networks. Plops Comput Biol 3:e17.

Achard S, Salvador R, Whitcher B, Suckling J, Bullmore E (2006): A resilient, low-frequency, small-world human brain functional network with highly connected association cortical hubs. J Neurosci 26:63–72.

Albert M, Knoefel J. 1994. Clinical Neurology of Aging. New York: Oxford University Press.

Bassett DS, Bullmore E (2006): Small-world brain networks. Neuroscientist 12:512–523.

Bassett DS, Meyer-Lindenberg A, Achard S, Duke T, Bullmore E (2006): Adaptive reconfiguration of fractal small-world human brain functional networks. Proc Natl Acad Sci USA 103:19518–19523.

Bassett DS, Bullmore E, Verchinski BA, Mattay VS, Weinberger DR, Meyer-Lindenberg A (2008): Hierarchical organization of human cortical networks in health and schizophrenia. J Neurosci 28:9239–9248.

Bergfield KL, Hanson KD, Chen K, Teipel SJ, Hampel H, Rapoport SI, Moeller JR, Alexander GE (2010): Age-related networks of regional covariance in MRI gray matter: Reproducible multivariate patterns in healthy aging. Neuroimage 49:1750–1759.

Bullmore E, Sporns O (2009): Complex brain networks: Graph theoretical analysis of structural and functional systems. Nat Rev Neurosci 10:186–198.

Bullmore ET, Suckling J, Overmeyer S, Rabe-Hesketh S, Taylor E, Brammer MJ (1999): Global, voxel, and cluster tests, by theory and permutation, for a difference between two groups of structural MR images of the brain. IEEE Trans Med Imaging 18:32–42.

Catani M, ffytche DH (2005): The rises and falls of disconnection syndromes. Brain 128:2224–2239.

Chen ZJ, He Y, Rosa-Neto P, Germann J, Evans AC (2008): Revealing modular architecture of human brain structural networks by using cortical thickness from MRI. Cereb Cortex 18:2374–2381.

Clauset A, Newman MEJ, Moore C (2004): Finding community structure in very large networks. Phys Rev E 70:66111.

Costa LdF, Rodrigues FA, Travieso G, Boas PRV (2007): Characterization of complex networks: A survey of measurements. Adv Phys 56:167–242.

Danon L, Duch J, Diaz-Guilera A, Arenas A (2005): Comparing community structure identification. J Stat Mech 9:P09008.

Eguiluz VM, Chialvo DR, Cecchi GA, Baliki M, Apkarian AV (2005): Scale-free brain functional networks. Phys Rev Lett 94:018102.

Fair DA, Cohen AL, Power JD, Dosenbach NU, Church JA, Miezin FM, Schlaggar BL, Petersen SE (2009): Functional brain networks develop from a "local to distributed" organization. PLoS Comput Biol 5:e1000381.

Ferrarini L, Veer IM, Baerends E, van Tol MJ, Renken RJ, van der Wee NJ, Veltman DJ, Aleman A, Zitman FG, Penninx BW, van Buchem MA, Reiber JH, Rombouts SA, Milles J (2009): Hierarchical functional modularity in the resting-state human brain. Hum Brain Mapp 30:2220–2231.

Ferri R, Rundo F, Bruni O, Terzano MG, Stam CJ (2007): Small-world network organization of functional connectivity of EEG slow-wave activity during sleep. Clin Neurophysiol 118:449–456.

Freeman LC (1977): A set of measures of centrality based on betweenness. Sociometry 40:35–41.

Friston KJ, Holmes AP, Worsley KJ, Poline JP, Frith CD, Frackowiak RSJ (1995): Statistical parametric maps in functional imaging: A general linear approach. Hum Brain Mapp 2:189–210.

Ge Y, Grossman RI, Babb JS, Rabin ML, Mannon LJ, Kolson DL (2002a): Age-related total gray matter and white matter changes in normal adult brain. Part I: volumetric MR imaging analysis. AJNR Am J Neuroradiol 23:1327–1333.

Ge Y, Grossman RI, Babb JS, Rabin ML, Mannon LJ, Kolson DL (2002b): Age-related total gray matter and white matter changes in normal adult brain. Part II: Quantitative magnetization transfer ratio histogram analysis. AJNR Am J Neuroradiol 23:1334–1341.

Genovese CR, Lazar NA, Nichols T (2002): Thresholding of statistical maps in functional neuroimaging using the false discovery rate. Neuroimage 15:870–878.

Girvan M, Newman MEJ (2002): Community structure in social and biological networks. Proc Natl Acad Sci USA 99:7821–7826.

Gong G, Rosa-Neto P, Carbonell F, Chen ZJ, He Y, Evans AC (2009a): Age- and gender-related differences in the cortical anatomical network. J Neurosci 29:15684–15693.

Gong G, He Y, Concha L, Lebel C, Gross DW, Evans AC, Beaulieu C (2009b): Mapping anatomical connectivity patterns of human cerebral cortex using in vivo diffusion tensor imaging tractography. Cereb Cortex 19:524–536.

Guimerà R, Amaral LAN (2005a): Functional cartography of complex metabolic networks. Nature 433:895–900.

Guimerà R, Amaral LAN (2005b): Cartography of complex networks: Modules and universal roles. J Stat Mech 2:P02001.

Guimerà R, Sales-Pardo M, Amaral LAN (2004): Modularity from fluctuations in random graphs and complex networks. Phys Rev E 70:25101.

Guimerà R, Mossa S, Turtschi A, Amaral LAN (2005): The worldwide air transportation network: Anomalous centrality, community structure, and cities' global roles. Proc Natl Acad Sci USA 102:7794–7799.

Hagmann P, Kurant M, Gigandet X, Thiran P, Wedeen VJ, Meuli R, Thiran JP (2007): Mapping human whole-brain structural networks with diffusion MRI. PLoS ONE 2:e597.

Hagmann P, Cammoun L, Gigandet X, Meuli R, Honey CJ, Wedeen VJ, Sporns O (2008): Mapping the structural core of human cerebral cortex. PLoS Biol 6:e159.

Hartwell LH, Hopfield JJ, Leibler S, Murray AW (1999): From molecular to modular cell biology. Nature 402:47–52.

He Y, Chen ZJ, Evans AC (2007): Small-world anatomical networks in the human brain revealed by cortical thickness from MRI. Cereb Cortex 17:2407–2419.

He Y, Chen ZJ, Evans AC (2008): Structural insights into aberrant topological patterns of large-scale cortical networks in Alzheimer's disease. J Neurosci 28:4756–4766.

He Y, Dagher A, Chen Z, Charil A, Zijdenbos A, Worsley K, Evans A (2009a): Impaired small-world efficiency in structural cortical networks in multiple sclerosis associated with white matter lesion load. Brain 132:3366–3379.

He Y, Wang J, Wang L, Chen ZJ, Yan C, Yang H, Tang H, Zhu C, Gong Q, Zang Y, Evans AC (2009b): Uncovering intrinsic modular organization of spontaneous brain activity in humans. PLoS One 4:e5226.

Hedden T, Gabrieli JDE (2004): Insights into the ageing mind: A view from cognitive neuroscience. Nat Rev Neurosci 5:87–96.

Iturria-Medina Y, Sotero RC, Canales-Rodriguez EJ, Aleman-Gomez Y, Melie-Garcia L (2008): Studying the human brain anatomical network via diffusion-weighted MRI and graph theory. Neuroimage 40:1064–1076.

Jean Talairach PT. 1988. Co-Planar Stereotaxic Atlas of the Human Brain. Stuttgart: Thieme.

Kamada T, Kawai S (1989): An algorithm for drawing general undirected graphs. Inform Process Lett 31:7–15.

Kashtan N, Alon U (2005): Spontaneous evolution of modularity and network motifs. Proc Natl Acad Sci USA 102:13773–13778.

Lancaster JL, Woldorff MG, Parsons LM, Liotti M, Freitas CS, Rainey L, Kochunov PV, Nickerson D, Mikiten SA, Fox PT (2000): Automated Talairach atlas labels for functional brain mapping. Hum Brain Mapp 10:120–131.

Latora V, Marchiori M (2001): Efficient behavior of small-world networks. Phys Rev Lett 87:198701.

Lerch JP, Worsley K, Shaw WP, Greenstein DK, Lenroot RK, Giedd J, Evans AC (2006): Mapping anatomical correlations across cerebral cortex (MACACC) using cortical thickness from MRI. Neuroimage 31:993–1003.

Li Y, Liu Y, Li J, Qin W, Li K, Yu C, Jiang T (2009): Brain anatomical network and intelligence. PLoS Comput Biol 5:e1000395.

Liu Y, Liang M, Zhou Y, He Y, Hao Y, Song M, Yu C, Liu H, Liu Z, Jiang T (2008): Disrupted small-world networks in schizophrenia. Brain 131:945–961.

Maldjian JA, Laurienti PJ, Kraft RA, Burdette JH (2003): An automated method for neuroanatomic and cytoarchitectonic atlas-based interrogation of fMRI data sets. Neuroimage 19:1233–1239.

Maldjian JA, Laurienti PJ, Burdette JH (2004): Precentral gyrus discrepancy in electronic versions of the Talairach atlas. Neuroimage 21:450–455.

Mechelli A, Friston KJ, Frackowiak RS, Price CJ (2005): Structural covariance in the human cortex. J Neurosci 25:8303–8310.

Mesulam MM (1998): From sensation to cognition. Brain 121:1013–1052.

Meunier D, Achard S, Morcom A, Bullmore E (2009a): Age-related changes in modular organization of human brain functional networks. Neuroimage 44:715–723.

Meunier D, Lambiotte R, Fornito A, Ersche KD, Bullmore ET (2009b): Hierarchical modularity in human brain functional networks. Front Neuroinformatics 3:37.

Micheloyannis S, Pachou E, Stam CJ, Vourkas M, Erimaki S, Tsirka V (2006): Using graph theoretical analysis of multi channel EEG to evaluate the neural efficiency hypothesis. Neurosci Lett 402:273–277.

Micheloyannis S, Vourkas M, Tsirka V, Karakonstantaki E, Kanatsouli K, Stam CJ (2009): The influence of ageing on complex brain networks: A graph theoretical analysis. Hum Brain Mapp 30:200–208.

Newman MEJ (2004): Fast algorithm for detecting community structure in networks. Phys Rev E 69:066133.

Newman MEJ (2006a): Modularity and community structure in networks. Proc Natl Acad Sci USA 103:8577–8582.

Newman MEJ (2006b): Finding community structure in networks using the eigenvectors of matrices. Phys Rev E 74:36104.

Newman MEJ, Girvan M (2004): Finding and evaluating community structure in networks. Phys Rev E 69:026113.

Pezawas L, Meyer-Lindenberg A, Drabant EM, Verchinski BA, Munoz KE, Kolachana BS, Egan MF, Mattay VS, Hariri AR, Weinberger DR (2005): 5-HTTLPR polymorphism impacts human cingulate-amygdala interactions: A genetic susceptibility mechanism for depression. Nat Neurosci 8:828–834.

Radicchi F, Castellano C, Cecconi F, Loreto V, Parisi D (2004): Defining and identifying communities in networks. Proc Natl Acad Sci USA 101:2658–2663.

Redies C, Puelles L (2001): Modularity in vertebrate brain development and evolution. Bioessays 23:1100–1011.

Reichardt J, Bornholdt S (2006): When are networks truly modular? Phys D 224:20–26.

Resnick SM, Pham DL, Kraut MA, Zonderman AB, Davatzikos C (2003): Longitudinal magnetic resonance imaging studies of older adults: a shrinking brain. J Neurosci 23:3295–3301.

Robinson PA, Henderson JA, Matar E, Riley P, Gray RT (2009): Dynamical reconnection and stability constraints on cortical network architecture. Phys Rev Lett 103:108104.

Salvador R, Suckling J, Coleman MR, Pickard JD, Menon D, Bullmore E (2005): Neurophysiological architecture of functional magnetic resonance images of human brain. Cereb Cortex 15:1332–1342.

Salvador R, Martíez A, Pomarol-Clotet E, Gomar J, Vila F, Sarró S, Capdevila A, Bullmore E (2008): A simple view of the brain through a frequency-specific functional connectivity measure. NeuroImage 39:279–289.

Sato K, Taki Y, Fukuda H, Kawashima R (2003): Neuroanatomical database of normal Japanese brains. Neural Netw 16:1301–1310.

Smith CD, Chebrolu H, Wekstein DR, Schmitt FA, Markesbery WR (2007): Age and gender effects on human brain anatomy: A voxel-based morphometric study in healthy elderly. Neurobiol Aging 28:1075–1087.

Sowell ER, Peterson BS, Thompson PM, Welcome SE, Henkenius AL, Toga AW (2003): Mapping cortical change across the human life span. Nat Neurosci 6:309–315.

Sowell ER, Thompson PM, Leonard CM, Welcome SE, Kan E, Toga AW (2004): Longitudinal mapping of cortical thickness and brain growth in normal children. J Neurosci 24:8223–8231.

Sporns O, Zwi J (2004): The small world of the cerebral cortex. Neuroinformatics 2:145–162.

Sporns O, Tononi G, Edelman GM (2000): Theoretical neuroanatomy: Relating anatomical and functional connectivity in graphs and cortical connection matrices. Cereb Cortex 10:127–141.

Sporns O, Honey CJ, Kotter R (2007): Identification and classification of hubs in brain networks. PLoS ONE 2:e1049.

Stam CJ, Jones BF, Nolte G, Breakspear M, Scheltens P (2007): Small-world networks and functional connectivity in Alzheimer's disease. Cereb Cortex 17:92–99.

Strogatz SH (2001): Exploring complex networks. Nature 410:268–276.

Supekar K, Musen M, Menon V (2009): Development of large-scale functional brain networks in children. PLoS Biol 7:e1000157.

Taki Y, Kinomura S, Sato K, Goto R, Kawashima R, Fukuda H (2009): A longitudinal study of gray matter volume decline with age and modifying factors. Neurobiol Aging: doi:10.1016/j.neurobiolaging.2009.05.003.

Tisserand DJ, van Boxtel MPJ, Pruessner JC, Hofman P, Evans AC, Jolles J (2004): A voxel-based morphometric study to determine individual differences in gray matter density associated with age and cognitive change over time. Cereb Cortex 14:966–973.

Tzourio-Mazoyer N, Landeau B, Papathanassiou D, Crivello F, Etard O, Delcroix N, Mazoyer B, Joliot M (2002): Automated anatomical labeling of activations in SPM using a macroscopic anatomical parcellation of the MNI MRI single-subject brain. Neuroimage 15:273–289.

Valencia M, Pastor MA, Fernández-Seara MA, Artieda J, Martinerie J, Chavez M (2009): Complex modular structure of large-scale brain networks. Chaos 19:023119.

van den Heuvel MP, Stam CJ, Kahn RS, Hulshoff Pol HE (2009): Efficiency of functional brain networks and intellectual performance. J Neurosci 29:7619–7624.

Van Essen DC (2005): A population-average, landmark- and surface-based (PALS) atlas of human cerebral cortex. NeuroImage 28:635–662.

Wang J, Wang L, Zang Y, Yang H, Tang H, Gong Q, Chen Z, Zhu C, He Y (2009a): Parcellation-dependent small-world brain functional networks: A resting-state fMRI study. Hum Brain Mapp 30:1511–1523.

Wang L, Zhu C, He Y, Zang Y, Cao Q, Zhang H, Zhong Q, Wang Y (2009b): Altered small-world brain functional networks in children with attention-deficit/hyperactivity disorder. Hum Brain Mapp 30:638–649.

Watts DJ, Strogatz SH (1998): Collective dynamics of "small-world" networks. Nature 393:440–442.

Zalesky A, Fornito A, Harding IH, Cocchi L, Yücel M, Pantelis C, Bullmore ET (2010): Whole-brain anatomical networks: Does the choice of nodes matter? NeuroImage 50:970–983.

Cardiovascular Engineering and Technology, Vol. 2, No. 4, December 2011 *(© 2011)* pp. 361–371
DOI: 10.1007/s13239-011-0053-7

BMES BIOMEDICAL ENGINEERING SOCIETY™ www.bmes.org

Design Method of Self-expanding Stent Suitable for Diverse Clinical Manifestation Based on Mechanical Properties

DAISUKE YOSHINO[1] and MASAAKI SATO[1,2]

[1]Department of Bioengineering and Robotics, Graduate School of Engineering, Tohoku University, 6-6-01 Aramaki-Aoba, Aoba, Sendai 980-8579, Japan; and [2]Department of Biomedical Engineering, Graduate School of Biomedical Engineering, Tohoku University, 6-6-01 Aramaki-Aoba, Aoba, Sendai 980-8579, Japan

(Received 7 March 2011; accepted 7 July 2011; published online 16 July 2011)

Associate Editor Leo Hwa Liang oversaw the review of this article.

Abstract—Stent placement has received a great deal of attention as a minimally invasive procedure for treating, for example, vascular stenotic lesions associated with coronary atherosclerosis. However, the long-term placement of stents can lead to the severe problem of in-stent restenosis in blood vessels. In-stent restenosis results from neointimal thickening from the hyperplasia of smooth muscle cells, caused by the stimulus of the force of the stent on the vascular wall. In the present study, a method to design a bare metal stent suitable for diverse clinical manifestation is proposed for lowering the risk of in-stent restenosis. The proposed method consists of a design method and a modification method. In the design method, a stent with mechanical properties sufficient to expand the stenotic part in a blood vessel is designed by applying the mechanical properties of the host blood vessel. The force on the vascular wall when inserting the designed stent is concentrated at both ends of the stent, and the force concentration provokes the hyperplasia of smooth muscle cells. As a result, the risk of in-stent restenosis increases. The modification method was introduced into the proposed method to solve the problem of force concentration. After modification, the force concentration at the stent ends was markedly relaxed. This new-generation stent has a nonuniform shape along its axial direction. Thus, the proposed method will enable us to provide a suitable stent with a lower risk of in-stent restenosis.

Keywords—Self-expanding stent, Shape design, In-stent restenosis, Mechanical property, Mechanical stimulus, Clinical manifestation, New-generation stent.

Address correspondence to Daisuke Yoshino, Department of Bioengineering and Robotics, Graduate School of Engineering, Tohoku University, 6-6-01 Aramaki-Aoba, Aoba, Sendai 980-8579, Japan. Electronic mail: yoshino@bml.mech.tohoku.ac.jp

INTRODUCTION

Stent placement has received a great deal of attention as a minimally invasive procedure for treating, for example, vascular stenotic lesions associated with coronary atherosclerosis. Recently, in-stent restenosis has become a severe problem in blood vessels with long-term stent placement. In-stent restenosis results from neointimal thickening in the blood vessel from the hyperplasia of smooth muscle cells caused by the mechanical stimulus of the stent to the vascular wall. The drug-eluting stent (DES) containing immunosuppressive agents is already in clinical use to resolve this problem.[13] Compared to a bare metal stent (BMS), the DES is considered to be more effective in preventing the development of restenosis. However, the DES does not help to improve the life prognosis or to prevent myocardial infarction.[1,9,10] It has also been reported that the DES, not the BMS, might cause deterioration in the life prognosis.[15] Depletion of the immunosuppressive agents is a concern for longer use. Furthermore, when using a DES, serious side effects due to these drugs must be considered. Although many reports state that the use of a DES prevents in-stent restenosis, few studies have investigated the prevention of in-stent restenosis by designing and modifying the BMS itself. The focus of most of these studies has been to improve or optimize the BMS.

The stent must have a radial stiffness sufficient to expand the stenotic part outward in the blood vessel. Simultaneously, it must be sufficiently flexible to conform to the vascular wall. Neither the symptom nor the blood vessel shape is always the same for every patient. Therefore, it is more important to design stents suitable for each unique symptom and vessel shape. Colombo *et al.*[4] made evaluations of stent

deliverability, scaffolding, accurate positioning, and so on, for an average lesion of the coronary artery. They proposed a guideline for use in determining a suitable stent. This guideline was based on clinical trials, and therefore, it was governed by the doctor's judgment. In addition, sometimes the best-suited stent cannot be used because a stent must be chosen from only from those that are commercially available.

In this paper, a method is proposed for designing a stent that has good mechanical properties to suit diverse clinical manifestation. Figure 1 shows the flow of the design process for such a stent. The first step is to determine the radial stiffness of the stent necessary for expanding the stenotic part in the blood vessel based on the patient's symptom information. Next, based on the determined radial stiffness and the sensitivities of the mechanical properties of the stent defined in our previous paper,[23] the design variables of a suitable stent are established. In the second stage of the design, which applies the modification method, the force on the vascular wall by insertion of the designed stent is evaluated by using the methods proposed by the authors.[24] This force is associated with the risk of in-stent restenosis. Next, based on the evaluation results, the designed stent is modified to be more suitable for that patient's symptom. After modification, the force on the vascular wall is evaluated again. The effect of shape modification is confirmed by comparing the forces on the vascular wall before and after the modifications. Finally, the modified stent shape is judged as a better stent shape. The details of this proposed design method are described in the following sections.

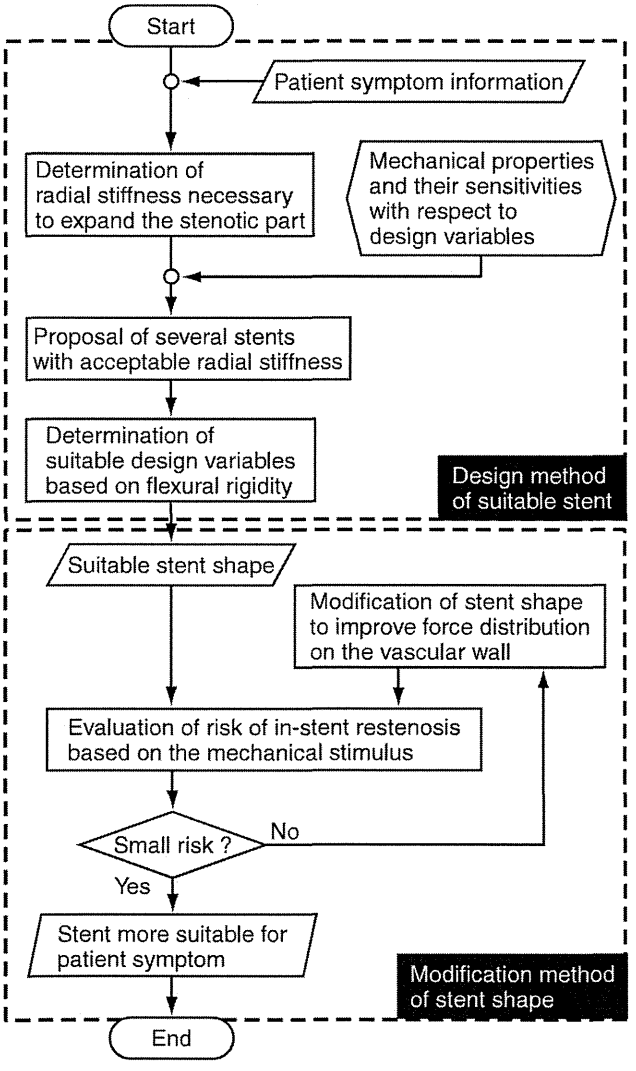

FIGURE 1. Flow of the stent design suitable for diverse clinical manifestation. The design consists of two steps. In the first stages, a stent to expand the stenotic part of a blood vessel is designed. In the second stage, the designed stent is modified to better suit the patient symptom information.

PREPARATION FOR A SUITABLE DESIGN

Mechanical Properties of the Target Stent

In the present study, we used the self-expanding SENDAI stent,[14] which is available for clinical use. Figures 2a and 2b show a photograph of the SENDAI stent and the two-dimensional shape, respectively.

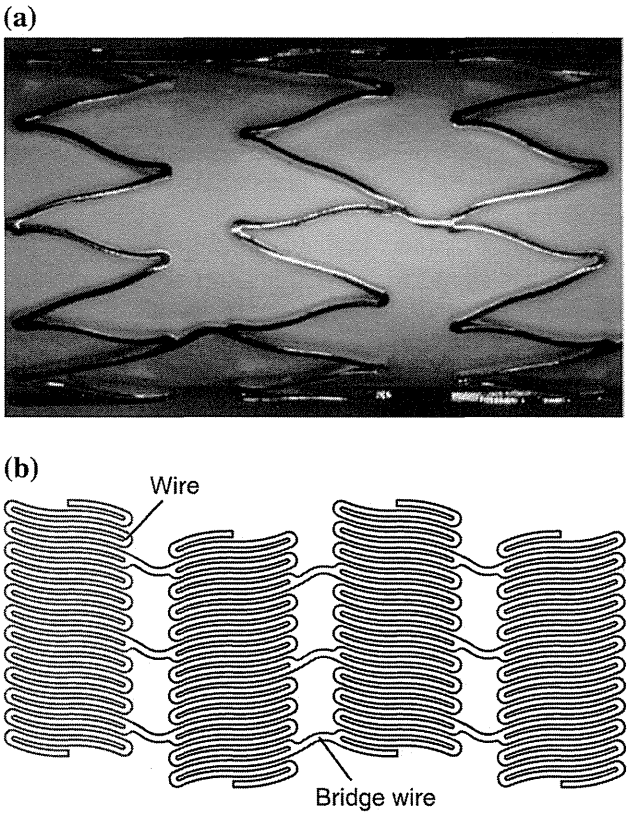

FIGURE 2. Self-expanding SENDAI stent used as the target stent: (a) photograph of the SENDAI stent 6 mm in diameter and (b) two-dimensional shape of the SENDAI stent.

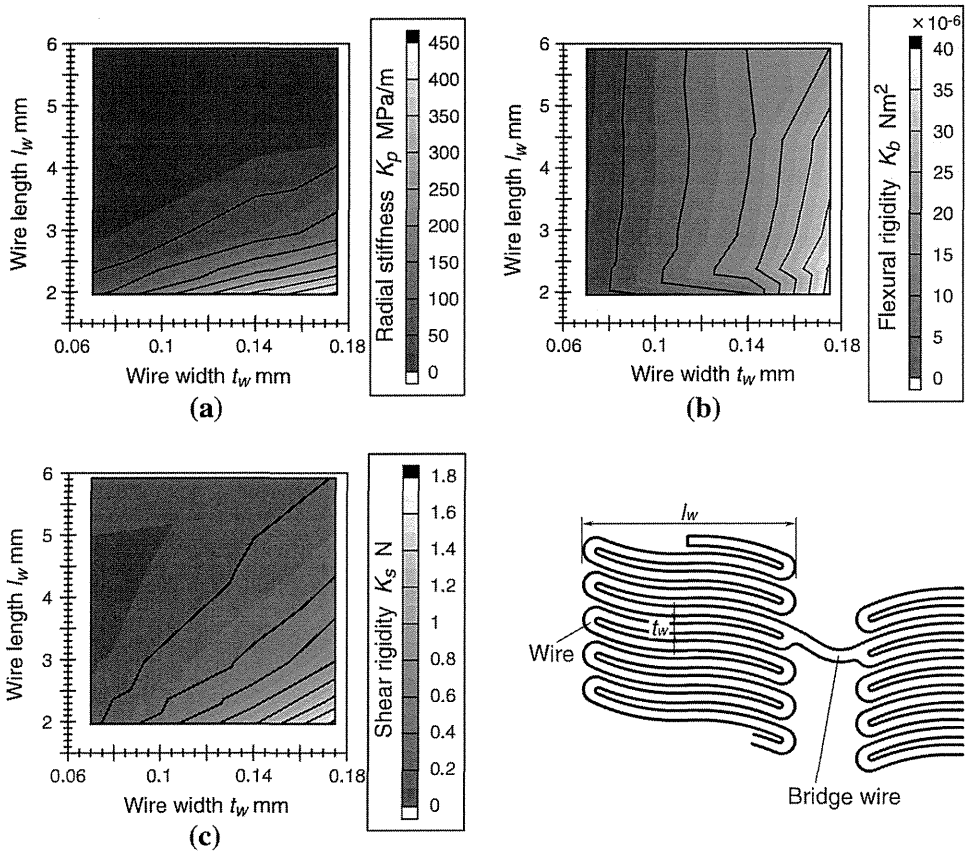

FIGURE 3. Sensitivities of the mechanical properties of the SENDAI stent 6 mm diameter to the design variables: (a) radial stiffness, (b) flexural rigidity, and (c) shear rigidity.

The wire section is constructed from 12 S-shaped wires. The strut section of the stent connects the wire sections through three bridge wires. The stent is made of a NiTi shape memory alloy.

We must know the relationship between the mechanical properties of a stent and the design variables in order to design a stent with specific properties. The mechanical properties of the SENDAI stent, such as radial stiffness, flexural rigidity, and shear rigidity, were evaluated, and their sensitivities to the design variables were also defined, as shown in Fig. 3.[23,24] The wire length along the axial direction and the wire width were selected as design variables. Isolines on the maps of mechanical properties are very important for proposing designs. The isoline is plotted onto the maps based on the required mechanical property, and design variables of the proposed design are determined from the isoline. In addition, we assumed the mechanical properties of the stent material as illustrated in Fig. 4: Young's modulus of 28 GPa, and Poisson's ratio of 0.3.

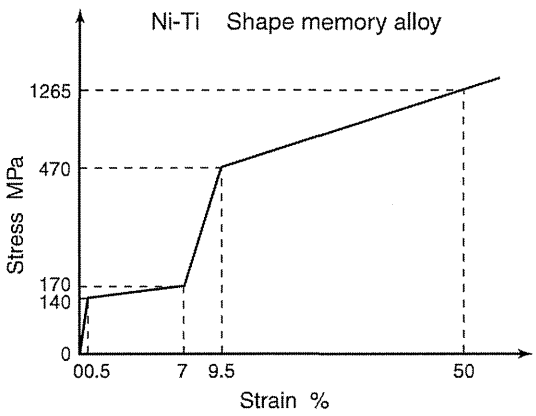

FIGURE 4. Assumed stress-strain relationship for the stent material.

Mechanical Properties of the Artery Model

When considering expanding the stenotic part in the blood vessel, as presented in Fig. 5, it is important to know the vascular mechanical properties. Arteries in a living body are always under internal pressure. Simultaneously, they are stressed by the strain produced along their axial direction by several tens of percent. In this sense, the vessel can be regarded as a thick cylinder in a multiaxial stress state. Therefore, a multiaxial stress test must be performed to measure the mechanical properties of blood vessels. However, this

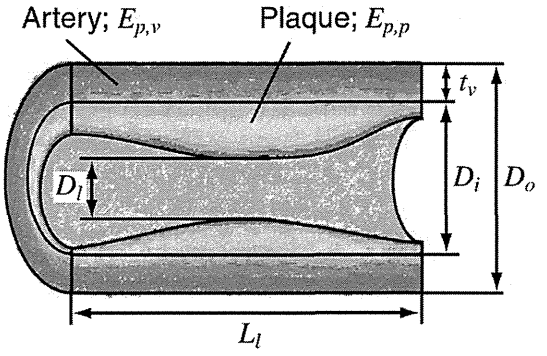

FIGURE 5. Dimensions of a blood vessel with stenosis.

is extremely difficult since there are many different types of blood vessels. In this study, the pressure strain elastic modulus proposed by Peterson *et al.*[16] was used because it is easy to manipulate. The pressure strain elastic modulus $E_{p,v}$ of a blood vessel can be expressed by the following equation

$$E_{p,v} = \frac{\Delta p}{\Delta D_o / D_o} \tag{1}$$

where D_o is the outer diameter of the blood vessel, and ΔD_o and Δp are the increase in the blood vessel diameter and the increase in the internal pressure, respectively. The pressure strain elastic modulus has been widely used in clinical studies (for example[18]), and many reports are available.

Another parameter that is often available for clinical use is the stiffness parameter β, which is used to express the apparent stiffness of the vascular wall.[8] This stiffness parameter is related to the pressure strain elastic modulus, and so they can be readily converted from one to the other, according to the equations

$$\ln \frac{p}{p_s} = \beta \left(\frac{D}{D_o} - 1 \right) \tag{2}$$

$$\begin{aligned} \frac{p_s + \Delta p}{p_s} &= \exp\left(\beta \frac{\Delta D_o}{D_o} \right), (p = p_s + \Delta p,\ D = D_o + \Delta D_o) \\ &= 1 + \beta \frac{\Delta D_o}{D_o} + \left(\beta \frac{\Delta D_o}{D_o} \right)^2 + \cdots \\ &\approx 1 + \beta \frac{\Delta D_o}{D_o} \end{aligned} \tag{3}$$

$$\begin{aligned} \beta &\approx \frac{\Delta p / (\Delta D_o / D_o)}{p_s} \\ &= \frac{E_{p,v}}{p_s} \end{aligned} \tag{4}$$

where p_s is the arbitrary standard internal pressure; p_s is set as 13.33 kPa (100 mmHg), which is within the normal physiological blood pressure range.

DESIGN METHOD OF A STENT HAVING SUITABLE MECHANICAL PROPERTIES TO EXPAND A STENOTIC ARTERY

Determination of the Radial Stiffness Necessary to Expand the Stenotic Part in an Artery

In addition to the pressure strain elastic modulus $E_{p,v}$ of the blood vessel, the parameters required to determine the radial stiffness of the stent necessary to expand the stenotic part in a blood vessel are the outer and inner diameters, D_o and D_i, of the blood vessel in the normal state; the minimum diameter D_l in the stenotic part, the length of the stenotic part L_l, and the pressure strain elastic modulus of the plaque $E_{p,p}$. Also required is the internal diameter after the treatment is carried out, D_t, which is a target indicator of the amount by which to improve the blood flow level at that location. Given all the values listed above, the calculations for the necessary radial stiffness are made as follows.

Since an increase in the diameter of a blood vessel corresponds to a circumferential strain on a cylinder, a blood vessel with stenosis can be modeled by simply using springs connected in parallel, as shown in Fig. 6. Thus, the internal pressure in blood vessel p^*, which is necessary to expand the stenotic part, can be obtained by

$$p^* = (E_{p,v} + E_{p,p}) \frac{D_t - D_l}{D_o} = E_{p,vl} \frac{D_t - D_l}{D_o}. \tag{5}$$

When measuring the pressure strain elastic modulus of the plaque $E_{p,p}$ is difficult, it is possible to replace the sum of the elastic moduli, $E_{p,v} + E_{p,p}$, by the pressure

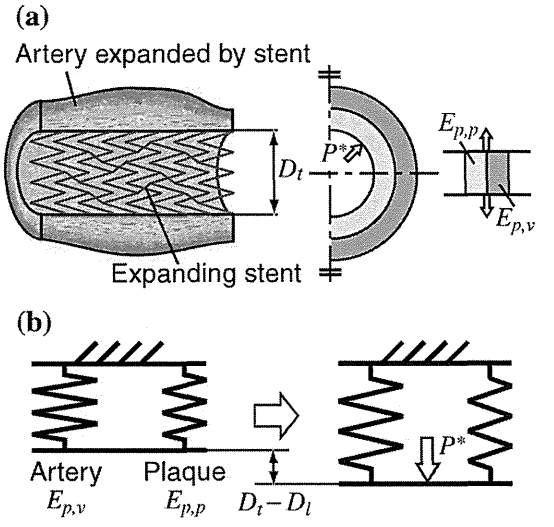

FIGURE 6. Simplified modeling of the expansion of the stenotic part in an artery by inserting a stent.

strain elastic modulus of the diseased blood vessel $E_{p,vl}$, which can be easily measured.

As a matter of fact, the diameter of the stent inserted into the stenotic part is greater than the target vascular diameter after treatment. Consequently, from the stent diameter d_s and the target vascular diameter D_t obtained after treatment, the radius reduction Δr in the stent after insertion can be calculated by the following equation:

$$\Delta r = \frac{d_s - D_t}{2}. \tag{6}$$

The radial stiffness K_p of the stent is defined as the ratio of the pressure p exerted on the outer surface of the stent in the radial direction to the radius reduction Δr of the stent, as follows[23]:

$$K_p = \frac{p}{\Delta r}. \tag{7}$$

By substituting Eqs. (5) and (6) into Eq. (7), the radial stiffness K_p^* necessary to expand the stenotic part is obtained as follows:

$$K_p^* = 2(E_{p,v} + E_{p,p})\frac{D_t - D_l}{D_o(d_s - D_t)} = 2E_{p,vl}\frac{D_t - D_l}{D_o(d_s - D_t)}. \tag{8}$$

The obtained K_p^* is the minimum stiffness required to expand the stenotic part in the blood vessel. Therefore, when designing a stent, the chosen stiffness should be greater than this K_p^* value.

Now consider the case where a stent with a diameter of 6 mm is inserted into a coronary artery. The symptoms shown in Table 1 are examples based on references.[5,12] Based on this data, the radial stiffness K_p^* necessary to expand the stenotic part in the blood vessel is calculated by Eq. (8) to be $K_p^* =$ 366.7 MPa/m.

The required radial stiffness K_p^* is plotted as a broken line on the radial stiffness map shown in Fig. 7. From this line, it is possible to determine the design variables for a stent with sufficient radial stiffness to expand the stenotic part of the blood vessel. Based on these, the designer can proceed to work with some design propositions.

Range of Selectable Flexural Rigidity and the Dilemma of Selecting the Design

After inserting an originally straight stent into a curved blood vessel and leaving it there, the stent generally conforms to the blood vessel shape. Nevertheless, because the flexural rigidity of the stent is greater than that of the blood vessel, the blood vessel tends to become straighter. This phenomenon of straightening of the blood vessel was previously described in detail, and a method to calculate the force

TABLE 1. Assumed patient symptom information.

Coronary artery	Parameters
Outer diameter, D_o (mm)	4.90
Inner diameter, D_i (mm)	4.06
Least diameter of lesion, D_l (mm)	2.5
Length of lesion, L_l (mm)	10
Total flexion angle (°)	90
(Flexion angle (°))	(45)
Rate of stenosis by ECST method (%)	38.4
Pressure strain elastic modulus of artery, $E_{p,v}$ (MPa)	0.602
Pressure strain elastic modulus of diseased artery, $E_{p,vl}$ (MPa)	0.628
Inner diameter after treatment, D_t (mm)	4.56

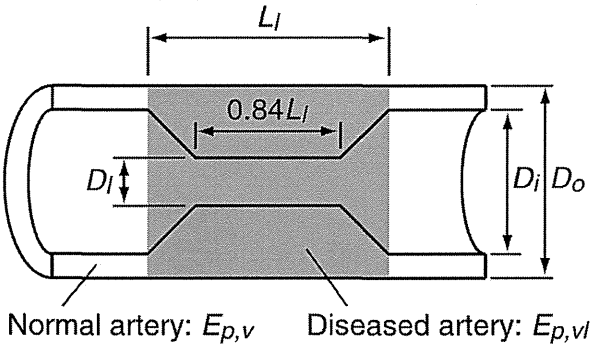

Schematic view of assumed symptom

resulting in the straightening of the blood vessel was proposed by the authors.[24] It is apparent that this force depends on the flexural rigidity of the stent, and that greater flexural rigidity results in a larger force. A force too large can damage the vascular wall. Consequently, it is important to choose the most appropriate flexural rigidity of the stent.

By plotting the proposed designs obtained from the required radial stiffness K_p^* on a flexural rigidity map, the broken line shown in Fig. 8a is obtained. For one radial stiffness value, multiple flexural rigidity values can be selected as long as they are within the range given in the figure.

When evaluating a possible risk of restenosis or blood vessel damage, the circumferential stress generated in the vascular wall is generally used. The

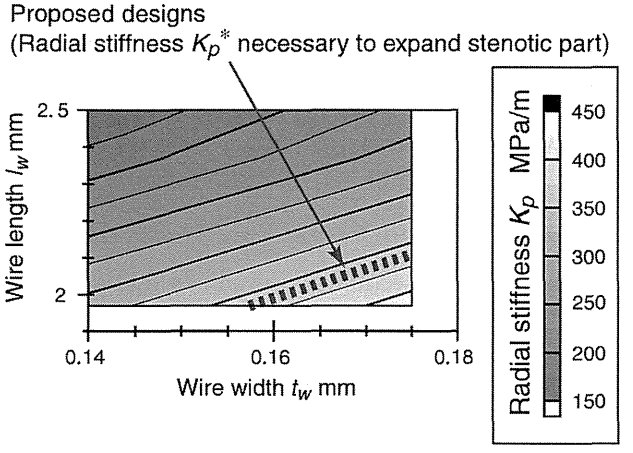

FIGURE 7. Proposed designs having the radial stiffness necessary to expand the stenotic part of a blood vessel. By assuming that a stent is inserted into a coronary artery, a value of 0.602 MPa was used for the pressure strain elastic modulus $E_{p,v}$ of the normal part of the coronary artery, and a value of 0.628 MPa for the pressure strain elastic modulus $E_{p,vl}$ of the diseased artery. For the coronary artery model, D_o = 4.90 mm, D_i = 4.06 mm, and D_l = 2.5 mm were assumed. The corresponding part of the map is magnified and displayed.

circumferential stress $\sigma_{\theta\theta}$ in the vascular wall can be defined using Laplace's law, as follows:

$$\sigma_{\theta\theta} = \frac{p_i D_i}{D_o - D_i} \tag{9}$$

where p_i is the internal pressure in the blood vessel. Bedoya *et al.*[2] suggested three critical stresses based on the circumferential stress. However, none of the limiting values for the circumferential stress, which might prevent damage on the vascular wall or neointimal thickening, are yet quantitatively available. Therefore, the flexural rigidity should be made smaller to decrease the force acting on the vascular wall. In other words, the designer should select the smallest flexural rigidity from the range of selectable values shown in Fig. 8a.

Figure 8b shows the stent shape designed in consideration of the rules described above. The designed stent is referred to as SDCO and has a wire length l_w^* of 2.01 mm, and a wire width t_w^* of 0.16 mm. In addition, the length of the designed stent is determined so that it occupies the blood vessel from the stenotic part to the normal part at each end in consideration of actual clinical use. The length of the SDCO is 22.0 mm (the stent consists of 8 wire sections and 7 strut sections). The flexural rigidity of the SDCO is $K_b^* = 25.1 \times 10^{-6}$ Nm^2. Similarly, the shear rigidity of the SDCO, based on the map of the rigidity, is $K_s^* = 1.33$ N.

Evaluation of the Risk of In-stent Restenosis Based on the Mechanical Stimulus

Figure 9 shows the distributions of the contact force and the straightening force when the SDCO is inserted into the coronary artery. These distributions were calculated by the previously proposed method.[24]

First, let us focus attention on the force on the vascular wall. Although the contact force is large at the stenotic part, the generation of this large force is unavoidable for expansion of the stenotic part.

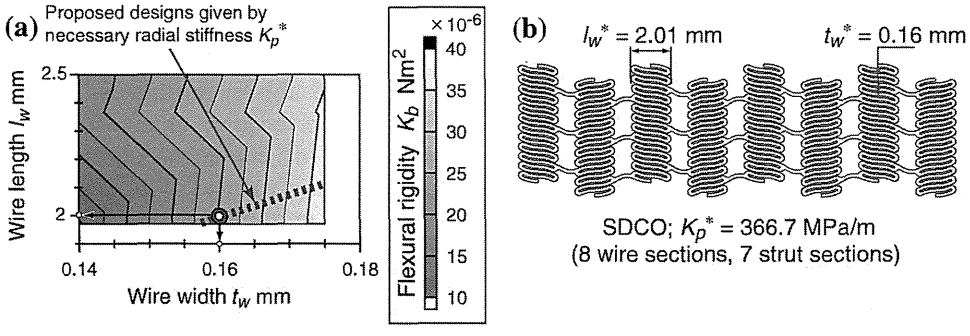

FIGURE 8. Selection of the proposed design from the viewpoint of flexural rigidity. (a) The selectable range of flexural rigidities is indicated by the broken line. The corresponding part of the map is magnified and displayed as in Fig. 6. (b) A stent 6 mm in diameter is designed to suit the assumed symptom of the coronary artery.

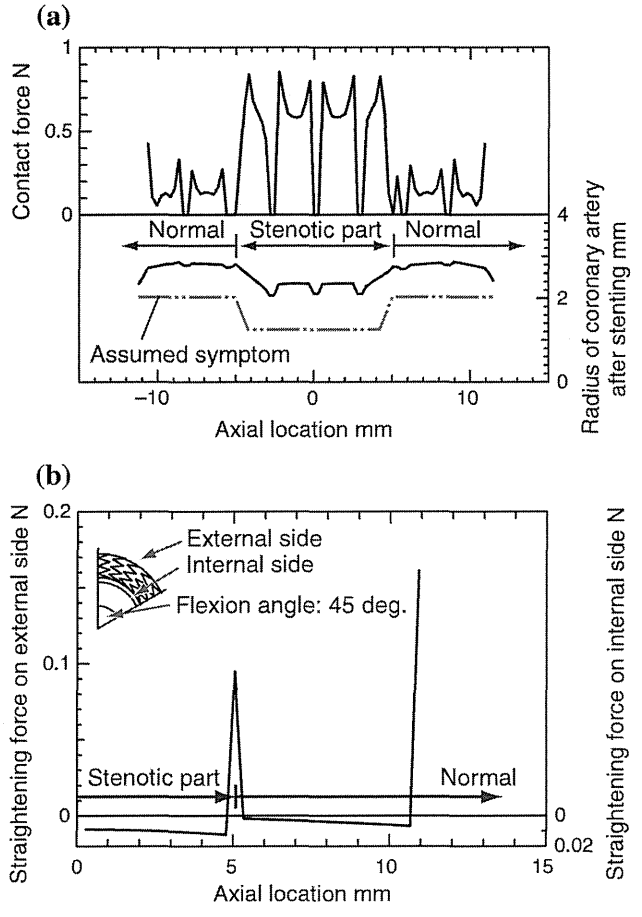

FIGURE 9. Computational results of forces which are exerted on the coronary artery wall by insertion of the SDCO. (a) The distribution of the contact force between the SDCO and the coronary artery (upside), and the radius of the coronary artery after stenting (downside). The dot-dashed line indicates the initial shape of the artery wall with the assumed symptom. (b) The distribution of the straightening force on the coronary artery wall by insertion of the SDCO. The rihght side of the distribution is displayed from a consideration of the geometrical symmetry.

The contact force is also concentrated at both ends of the stent. The straightening force on the vascular wall is concentrated at the end of the stenotic part in addition to both ends of the stent.

It has been reported that the hyperplasia of smooth muscle cells and the neointimal proliferation occur at the stented part of an artery.[3,6] It is assumed that the hyperplasia and proliferation are caused by the mechanical stimulus acting on the vascular wall due to insertion of the stent. Schweiger *et al.*[17] reported that in-stent restenosis occurred primarily at both ends of the stent during the period 1–3 months after stenting. In the study of Lal *et al.*,[11] the majority of patients in the target patient population showed in-stent restenosis at the stent ends. Yazdani and Berry[22] cultured a stented native porcine carotid artery under physiologic pulsatile flow and pressure conditions for a week. They confirmed that the proliferation of smooth muscle cells occurred significantly at both ends of the stent. By summarizing these reports and evaluation results of the forces on the vascular wall, it is concluded that the force concentration provokes neointimal thickening due to the hyperplasia of smooth muscle cells, *i.e.*, in-stent restenosis.

Next, the expansion of the vascular wall is examined. The normal part of the artery is expanded to become much larger than the target diameter. This excessive expansion causes expansion of the entire stented part. As a result, stagnation and vortices of blood flow are induced, further increasing the potential for stent thrombosis.

The designed stent has mechanical properties sufficient to expand the stenotic part of the artery, but is not suitable for the normal part of the artery. Thus, it requires modification.

EFFECTIVE METHOD TO MODIFY THE STENT SHAPE IN CONSIDERATION OF THE RISK OF IN-STENT RESTENOSIS

Design Objective for the Shape Modification

In the previous section, it was shown that although a stent suitable for the assumed symptoms could be designed using the proposed design method, further modifications were still required. Two kinds of design objectives are set up for shape modification.

Objective for the Mechanical Stimulus

As shown in Fig. 9, the contact force on the normal part of the artery is concentrated at both ends of the stent. This force concentration provokes neointimal thickening from the hyperplasia of smooth muscle cells. Therefore, the contact force must be reduced at both ends of the stent. However, this force should be larger than a certain limit so that stent functions on the lesion.

Objective for the Blood Flow

As stated above, the normal part of the artery is expanded to become much larger than the target diameter. This expansion state of the artery causes stagnation and vortices of blood flow. As a result, stent thrombosis may be induced. Srinivas *et al.*[19] focused on the blood flow to optimize a coronary stent shape. They changed the strut shape and the spacing between the struts, and evaluated the vorticity, recirculation, and reattachment of the blood flow. As is shown in this study, it is very important to reduce stagnation and

vortex creation to decrease the risk of stent thrombosis. Therefore, the vascular wall should be expanded flatly by the insertion of the stent. The flat expansion of the artery can prevent the generation of stagnation and vortices in the stented artery.

Modification Method of the Stent Shape to Suit the Clinical Manifestation

The stent designed in the previous section has a uniform radial stiffness K_p^* along its axial direction. The radial stiffness K_p^* causes excessive expansion at the normal part of the artery because K_p^* was calculated for expansion of the stenotic part, which is generally stiffer than the normal part. The objective for the mechanical stimulus can be attained by decreasing the radial stiffness to a value corresponding to that of a normal artery. At the same time, the objective for blood flow must be attained. Therefore, the stent should have a radial stiffness K_p^{**} to expand the vascular wall at normal part only for the stent thickness t. This can achieve the flat expansion of the artery. By changing the stent radial stiffness at the normal part from K_p^* to K_p^{**}, the contact force can also decrease. In this study, it was decided to adopt the radial stiffness K_p^{**} as a compromise between the two design objectives.

The methods using the influence matrix described in our previous paper[24] are used for the shape modification. Figure 10 shows the concept for modification of the stent shape. The distributed contact force P_i^* on the stenotic part can be calculated based on the radial stiffness K_p^*, as follows:

$$P_i^* = \frac{\pi D_t K_p^* \Delta r_t l_w^*}{n_{CP}} \tag{10}$$

where D_t is the inner diameter of the blood vessel after treatment, Δr_t is the increase in the vascular radius of the target, l_w^* is the wire length of the stent designed based on the radial stiffness K_p^*. Also, n_{CP} represents the number of calculation points on the wire section. For simplicity, it was assumed that a uniform contact force was exerted on the vascular wall.

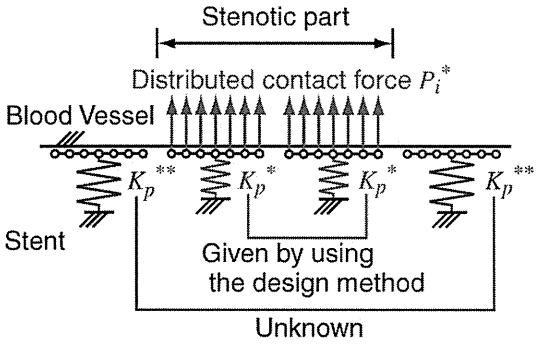

FIGURE 10. Concept for modification of the stent shape. The distributed contact force is obtained from the radial stiffness of the stent on the stenotic part by using the design method. The force that should be applied on the normal artery is calculated by using the obtained distributed contact force on the stenotic part.

As described in our previous paper,[24] the radial displacement of the vascular wall $\{r^{(v)}\} = (r_1^{(v)}, r_2^{(v)}, \ldots, r_n^{(v)})^T$ due to the unknown contact force $\{P\} = (P_1, P_2, \ldots, P_n)^T$ is given as follows:

$$[C^{(v)}]\{P\} = \{r^{(v)}\}, \tag{11}$$

where $[C^{(v)}]$ is the influence matrix of the blood vessel, defined by the radial displacement of the vascular wall due to the unit radial force. The calculated contact force P_i^* is substituted into Eq. (11), and the influence matrix $[C^{(v)}]$ is downsized to the matrix $[C^{(v)}_{\text{normal}}]$ of the normal blood vessel.

$$[C^{(v)}_{\text{normal}}]\{P^{**}\} = \{r^{(v)}_{\text{normal}}\} + [C^{(v)}_{\text{stenosis}}]\{P^*\} \tag{12}$$

$[C^{(v)}_{\text{stenosis}}]$ is the influence matrix of the stenotic part, and $\{r^{(v)}_{\text{normal}}\}$ is the radial displacement of the normal part of the blood vessel wall. Equation (12) is solved for $\{P^{**}\}$ to obtain the distributed force P_i^{**} that can expand the normal part to the stent thickness t.

Here, it is assumed that the wire length after modification is l_w^{**} and the calculation points from k to l are included in the modified wire section. The required radial stiffness K_p^{**} is defined as follows:

$$K_p^{**} = \frac{\sum_{i=k}^{l} P_i^{**}}{\pi D_t l_w^{**} t}. \tag{13}$$

The K_p^{**} value calculated by Eq. (13) is plotted on the radial stiffness map. As a result, the wire width t_w^{**} after modification is determined from the l_w^{**} value and the curve of K_p^{**} on the map. Therefore, the designed stent has to be modified to the shape of l_w^{**} and t_w^{**} at the normal part of the blood vessel. Considering that an increase in the stent length is undesirable, the designer should keep the wire length l_w^{**} equal to l_w^* after the modification. However, it is possible that the wire width t_w^{**} after the modification cannot be obtained because of the mismatch between the assumed l_w^{**} value and the curve of K_p^{**}. In this case, the designer can increase the wire length l_w^{**}, perform the same procedures, and determine the l_w^{**} and t_w^{**} values.

The required radial stiffness K_{p1}^{**} at both ends of the SDCO is 50.3 MPa/m. The radial stiffness K_{p2}^{**} at the normal part of the artery except for both stent ends is also calculated as 155.2 MPa/m. From the dot-dashed curves of K_{p1}^{**} and K_{p2}^{**} shown in Fig. 11a, it is determined that l_{w1}^{**} is 2.52 mm, t_{w1}^{**} is 0.087 mm, l_{w2}^{**} is 2.01 mm, and t_{w2}^{**} is 0.094 mm. Figure 11b shows the modified shape of the SDCO.

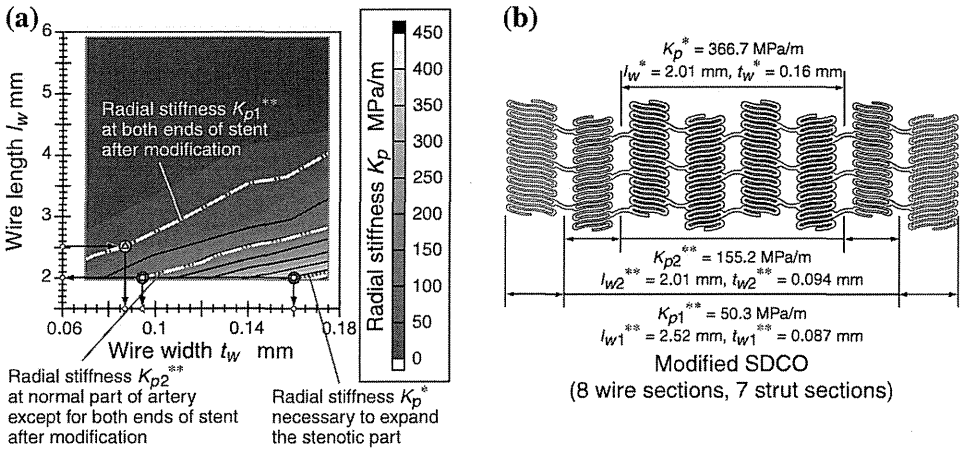

FIGURE 11. The SDCO stent 6 mm in diameter is modified to suit the assumed symptom of the coronary artery. (a) Design variables after modification are determined by using the map of the radial stiffness. (b) The modified SDCO has a nonuniform shape along its axial direction.

The flexural rigidity K_{b1}^{**} at both ends of the SDCO is 5.75×10^{-6} Nm^2, and the shear rigidity K_{s1}^{**} is 0.20 N. At the normal part of the artery except for both stent ends, the flexural rigidity K_{b2}^{**} of the SDCO is 6.00×10^{-6} Nm^2, and the shear rigidity K_{s2}^{**} is 0.42 N.

Confirmation of the Effect of the Shape Modification

Figure 12 shows a comparison of the force on the vascular wall by insertion of the stent before and after the modifications. After the modifications of the SDCO, an approximately 80% reduction in the concentrated contact force was attained (Fig. 12a). Furthermore. the concentrated straightening force at the stent ends after modification was reduced to approximately 35% of that before modification of the SDCO (Fig. 12b).

On the other hand, it is recognized that straightening force increases at the stenotic-healthy tissue interface (the axial location is 5 mm in Fig. 12b). The concentration of straightening force also occurs at the axial location of 8 mm. After modification of the stent shape, the flexural and shear rigidities of the stent vary with the axial location. The bending state of the stent changes at the changing point of the rigidities, which corresponds to the turn of the stent shape. Therefore, straightening force increases due to changing of the stent bending state based on rigidities changing. Although the risk of the vessel rupture slightly increases at the stenotic-healthy tissue interface, it is achieved that the straightening force is significantly reduced at both ends of the stent, where the hyperplasia of smooth muscle cells is frequently reported.

The modified stent can expand the vascular wall in a more flat manner. Therefore, modification of the designed stent by using the proposed method can relax

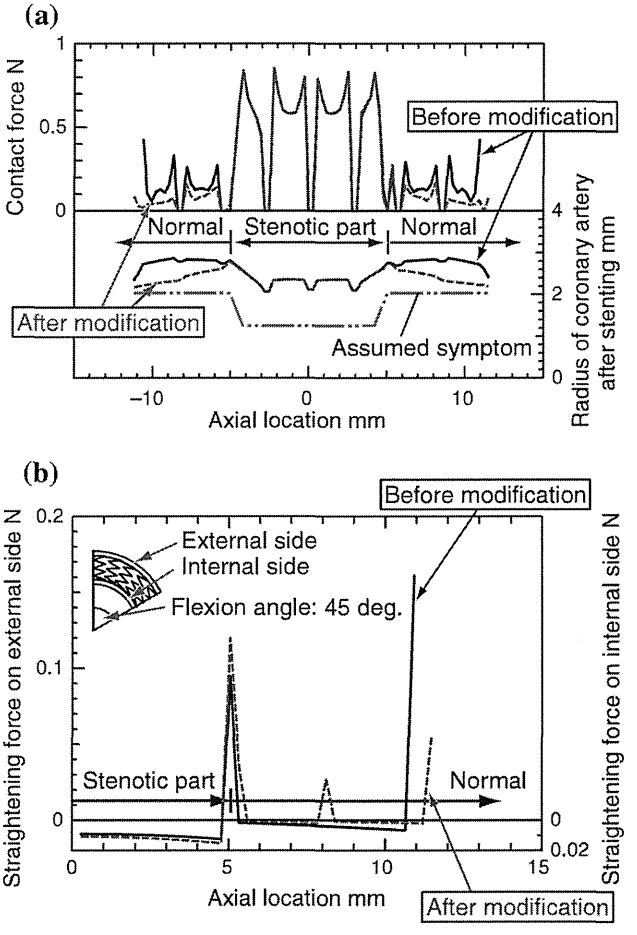

FIGURE 12. Confirmation of the effect of shape modification: (a) the contact force between the SDCO and the coronary artery (upside), and the radius of the coronary artery after stenting (downside). The dot-dashed line indicates the initial shape of the artery wall with the assumed symptom. (b) The straightening force on the coronary artery wall by insertion of the SDCO.

the force concentration at both ends of the stent by attaining flat expansion of the vascular wall.

EVALUATION AND DISCUSSION OF THE VALIDITY OF THE DESIGN METHOD

Based on the research of Yazdani and Berry[22] and the evaluation of the force on the vascular wall, it was decided that the force concentration at the stent ends influences the hyperplasia of smooth muscle cells. Gu *et al.*[7] calculated the von Mises stress generated by insertion of the stent. They also evaluated the relationship between the stress in the coronary artery and the rate of in-stent restenosis. Their evaluation results showed that the rate of in-stent restenosis increases with the increase of stress in the artery. Therefore, decreasing the force on the vascular wall at both ends of the stent prevents the hyperplasia of smooth muscle cells and reduces the rate of in-stent restenosis. Using the design method proposed in this paper, a suitable stent can be designed. The design method has the ability to relax the force concentration at the stent ends without losing the ability to expand the stenotic part.

Schweiger *et al.*[17] reported that in-stent restenosis occurred mostly in the part distant from the stent end or in the extended area of the stented part during the period 3–12 months after stenting. The details of the mechanical factors for this later occurrence of in-stent restenosis are still unclear. Several studies found that delayed neointimal proliferation comes into balance with the continuous expansion of the self-expanding stent.[3] Therefore, compared with early-stage neointimal thickening at the stent ends, this delayed neointimal proliferation is not as great a concern.

The problem when designing stents is whether the symptom information can actually be obtained. The shape and dimensions of the lesion can be measured by using computed tomography (CT) angiography. It is assumed that measuring the pressure strain elastic modulus of the artery in a living body is the most difficult. However, the method proposed by the research team at Tohoku University[20,21] enabled us to measure the elastic modulus of the artery in a living body.

Based on the evaluation and discussion presented above, the validity of the proposed design method is confirmed. Consequently, a stent with a low risk of in-stent restenosis can be provided by designing and modifying the shape of the BMS itself.

CONCLUSION

In this paper, a method was proposed for designing a stent suitable for diverse clinical manifestation. The proposed method consists of both the design method and the modification method. The design method enables us to design a stent with mechanical properties sufficient to expand the stenotic part of an artery. Using the modification method, we can relax the force concentration at the stent ends to avoid early-stage neointimal thickening. The stent designed by using the proposed method has nonuniform structures along its axial direction. This designed stent shape is radically new compared with the conventional stent shape that is uniform along its axial direction. Thus, the stent shape designed by using the method is considered to be a new-generation type.

REFERENCES

[1]Babapulle, M. N., L. Joseph, P. Bélisle, J. M. Brophy, and M. J. Eisenberg. A hierarchical Bayesian meta-analysis of randomised clinical trials of drug-eluting stents. *Lancet* 364:583–591, 2004.

[2]Bedoya, J., C. A. Meyer, L. H. Timmins, M. R. Moreno, and J. E. Moore, Jr. Effects of stent design parameters on normal artery wall mechanics. *J. Biomech. Eng.* 128:757–765, 2006.

[3]Clark, D. J., S. Lessio, M. O'Donoghue, C. Tsalamandris, R. Schainfeld, and K. Rosenfield. Mechanisms and predictors of carotid artery stent restenosis—a serial intravascular ultrasound study. *J. Am. Coll. Cardiol.* 47:2390–2396, 2006.

[4]Colombo, A., G. Stanlovic, and J. W. Moses. Selection of coronary stents. *J. Am. Coll. Cardiol.* 40:1021–1033, 2002.

[5]Gow, B. S., and C. D. Hadfield. The elasticity of canine and human coronary arteries with reference to postmortem changes. *Circ. Res.* 45:588–594, 1979.

[6]Grewe, P. H., T. Deneke, A. Machraoui, J. Barmeyer, and K.-M. Müller. Acute and chronic tissue response to coronary stent implantation: pathologic findings in human specimen. *J. Am. Coll. Cardiol.* 35:157–163, 2000.

[7]Gu, L., S. Zhao, A. K. Muttyam, and J. M. Hammel. The relation between the arterial stress and restenosis rate after coronary stenting. *J. Med. Devices* 4:31005-1-7, 2010.

[8]Hayashi, K., H. Handa, S. Nagasawa, A. Okumura, and K. Moritake. Stiffness and elastic behavior of human intracranial and extracranial arteries. *J. Biomech.* 13:175–184, 1980.

[9]Kastrati, A., J. Mehilli, J. Pache, C. Kaiser, M. Valgimigli, H. Kelbaek, M. Menichelli, M. Sabaté, M. J. Suttorp, D. Baumgart, M. Seyfarth, M. E. Pfisterer, and A. Schömig. Analysis of 14 trials comparing sirolimus-eluting stents with bare-metal stents. *N. Engl. J. Med.* 356:1030–1039, 2007.

[10]Lagerqvist, B., S. K. James, U. Stenestrand, J. Lindbäck, T. Nilsson, and L. Wallentin. Long-term outcomes with drug-eluting stents vs. bare-metal stents in Sweden. *N. Engl. J. Med.* 356:1009–1019, 2007.

[11]Lal, B. K., E. A. Kaperonis, S. Cuadra, I. Kapadia, and R. W. Hobson, II. Patterns of in-stent restenosis after carotid artery stenting: classification and implications for long-term outcome. *J. Vasc. Surg.* 46:833–840, 2007.